PERGAMON

International Journal of Multiphase Flow 28 (2002) 1479–1495

International Journal of Multiphase Flow

www.elsevier.com/locate/ijmulflow

A parametric model for evaporating liquid jets in dilute gas–solid flows

C. Zhu [a,*], G.L. Liu [a], X. Wang [a], L.-S. Fan [b]

[a] *Department of Mechanical Engineering, New Jersey Institute of Technology, Newark, NJ 07102, USA*
[b] *Department of Chemical Engineering, Ohio State University, Columbus, OH 43210, USA*

Received 8 February 2001; received in revised form 30 May 2002

Abstract

A parametric model has been developed for the study of liquid jet evaporation in gas–solid suspension flows. The model takes into account the phase interactions with phase changes in the mass, momentum and energy conservation equations of all the gas, liquid, and solid phases. Parametric effects on the mixing characteristics such as evaporation length, temperature and velocity of each phase, trajectories, and the phase volume fraction distributions are illustrated. It is found that the evaporation length is shortened in the presence of particles in a liquid jet of any injection angle. The evaporation length decreases with the increase of solids loading as well as the increase of jetting angle from co-current to counter-current. Comparison of jet evaporation length between the previously reported experimental results and modeling predictions shows a good qualitative agreement.

Keywords: Parametric model; Evaporating jet; Gas–solid flows

1. Introduction

Evaporating liquid jets into gas–solid suspension flows are frequently encountered in chemical processing industry, petroleum industry, power generation industry and other engineering fields. The rapid evaporation of liquid jets in a gas–solid flow can have significant effects on the gas–solid mixing near the jet nozzle regions. Typical effects of evaporating jets on gas–solid dynamics include the change of velocity of both gas and solids phases, dilution effect on solids concentration,

* Corresponding author. Tel.: +1-973-642-7624; fax: +1-973-642-4282.
E-mail address: zhu@adm.njit.edu (C. Zhu).

0301-9322/02/$ - see front matter © 2002 Published by Elsevier Science Ltd.
PII: S0301-9322(02)00038-1

temperature reduction of all phases and hence the reduction in reaction rate, and particle agglomeration or clustering. On the other hand, the particle loading (i.e., volumetric percentage of solid particles) in the gas–solid flow can also significantly change the jet structures such as jet evaporation region, evaporation rate, and collision frequency among droplets and solids. Recent experimental studies illustrate a significant effect of particle loading on the jet evaporation in the gas–solid pipe flows (Zhu et al., 2000).

Flow mixing by jet enhancement can be found in a co-current, counter-current, cross-flow, or oblique-flow arrangement. In cases where the jet and main flow stream become multiphase in nature, the jet enhanced mixing becomes more complicated than single phase mixing due to the phase interactions involved. The challenging factor is further increased when phase changes due to evaporation, condensation and chemical reaction are coupling with the multiphase mixing. A parametric model on jet enhanced mixing is aimed to understand the effect of key flow parameters on the mixing based upon the fundamental transport processes and principal phase-interactions.

Studies on gas and particle entrainment in turbulent jets can be dated back to the early 1960s. Field (1963) performed an extensive study of effects of particles on the entrainment of gas into free jets. Using an experimental apparatus similar to the one developed by Ricou and Spalding (1961), Field (1963) found that the presence of particles could increase the rate of entrainment, depending on the properties of the particle, the gas flow rate, and diameter of the initial jet. Platten and Keffer (1968) studied an air jet injected normally into cross-flows and hence proposed an empirical equation to estimate the gas entrainment velocity. Subramanian and Ganesh (1982, 1984) and Subramanian and Venkatram (1985) investigated the effects of particles on gas entrainment in axisymmetric jets. They reported that the presence of particles could reduce the amount of entrainment into a free jet as the particle loading increased. Tatterson et al. (1987) attributed the particle effect on free jet entrainment to a ratio of particle stopping distance to nozzle diameter. They suggested that, when the ratio is less than 3, the gas entrainment increases due to the presence of particles, while for the ratio between 3 and 65, the entrainment decreases. For ratios over 65, the presence of particles in the jet has no effect on the gas entrainment.

Many experimental studies on other characteristics of multiphase jet flows have been reported. Edelman et al. (1971) used the photographic method to study the particle trajectories when graphite particle of 1–5 μm in diameter were injected into a supersonic flow at a loading ratio up to 0.7. They showed that the centerlines of the particles and of the carrier gas nearly coincide with each other. Rudinger (1975) used a laser-Doppler system to study the flow behaviors of gas–solid jets in a cross-flow. The jet was a mixture of nitrogen and 33-μm glass beads with a mass-loading ratio between 2.3 and 25. The injection velocity of the particles was found to lie between 45% and 65% of the gas velocity at the jet exit. Measurements indicated that the particles are transported by carrier gas to an effective injection point where they separate from the carrier gas and then continue to move under the influence of their inertia and the viscous drag exerted by the cross-flow. Salzman and Schwartz (1978) used 15 μm silicate particles in airflow at loading ratios between 11 and 23. They defined the centerline as the locus of maximum particle concentration, which was determined by isokinetic sampling. Chen et al. (1994) developed a multifunction, multipurpose PIV system to study the droplet motion of a liquid jet in a high-speed cross-flow environment. Wu et al. (1998) investigated the structure of spray plumes from 0.5-mm water jets into a subsonic cross-flow. It was found that the liquid mass distribution depends on the liquid/air

momentum flux ratio. More large droplets are distributed toward the upper portion of the spray plume for large liquid/air momentum flux ratios, while for small momentum flux ratios, the large droplets are found in the central portion of the spray plume. They also suggested that the spray evaporation, spray width and evaporation-to-width ratio also increase with the momentum flux ratio.

Studies on parametric models of jet flows have also been actively pursued. However, most parametric models are restricted to the discussion of single-phase jet characteristics. Extensive reviews on single-phase jets were summarized by Abramovich (1963) and Rajaratnam (1976), respectively. Platten and Keffer (1968) suggested a parametric model on cross-flow jet in single-phase flows. In their model, it was assumed that the momentum of the jet perpendicular to the cross-stream is preserved, while the momentum of the jet along the cross-stream is increased by the momentum from the fluid entrainment. Campbell and Schetz (1973) investigated the cross-flow jet mixing of non-isothermal flows and further proposed a trajectory model to account for the effects of drag force, axial pressure gradient, entrainment, and heat losses of the jet flow. Forney and Kwon (1979) proposed a similarity law for the jet evaporation and mixing in turbulent pipe flows. The similarity is based on approximate solutions to the governing equations of a turbulent jet normal to a cross-flow. D'souza and Forney (1990) studied the effect of chemical reaction on the mixing of a turbulent jet in a laminar cross-flow. Li and Karagozian (1990) proposed a simple analysis to estimate the liquid jet-breakup location in a supersonic flow. Han and Chung (1992a) developed a parametric model on a premixed gas–solid suspension jet into a cross-flow of gas. Effect of the particle-to-gas velocity ratio at jet exit on the jet mixing is investigated. Han and Chung (1992b) further extended their model to investigate the jet mixing of a hot gas–solid jet into a cold cross-flow. Based on the model, effects of the non-uniformity in cross-flow velocity and heat transfer characteristics are revealed.

Several studies on evaporating liquid jets in gas–solid flows have been recently reported. Skouby (1998) used sampling probes to measure the catalyst concentration, mass flux and particle velocities of mixing flows in a riser with FCC catalyst and liquid nitrogen feed jets. Newton (1998) applied the X-ray imaging technique to study the direct liquid injection into a fluidized bed. In a computational approach, Chang et al. (1998) simulated a FCC process in which preliminary behaviors of heat transfer, multi-phase flows, droplet evaporation, and mixing by a jet flow were investigated. Zhu et al. (2000) reported an experimental study on liquid nitrogen spray jet into a gas–solid pipe flow. It was found that the liquid nitrogen spray length was significantly reduced by the increase of the particle loading. A similarity model was later developed for co-current jet mixing to interpret the experimental findings (Zhu et al., 2001). However, for the sake of simplicity, the similarity model excluded the phase interactions due to the velocity differences of phases.

The objective of this paper is to develop a general parametric model for applications of an evaporating liquid jet into a gas–solid suspension flow, which takes into account of the phase interactions with phase changes in all three phases. The model is focused on the study of the effects of jet parameters on the mixing characteristics such as droplet evaporation length, temperature and velocity of each phase, trajectories, and the phase volume fraction distributions. The governing equations are based on the conservation principles of mass, momentum and energy of all three phases. The computation results of the parametric model are in a good qualitative agreement with the experimental measurements.

2. Parametric modeling approach

Let us consider a case where a cold vapor–droplets jet is mixed with a hot gas–solid suspension flow at an injection angle of θ_0, as shown in Fig. 1. Major parameters of interest include ambient velocities and temperature of gas and solids, solid particle diameter, ambient volume fraction of solids, ambient pressure, injection velocities of vapor and droplets, injection angle, initial droplet size and droplet volume fraction, initial jet temperature, inlet area of jet, and physical properties of phases, such as specific heat and density.

It is assumed that a thermal equilibrium has been maintained between solids and carrying gas in the ambient gas–solid flow, and an initial thermal equilibrium is reached between vapor and droplets before the injection. In the jet region, the gas–vapor phase is perfectly mixed and behaves like an ideal gas. The centerline trajectory of gas–vapor mixture always coincides with the centerline of the liquid spray, which is true when the sizes of droplets and solids are small and particle loading is light. In addition, all phases are assumed to be symmetric to this centerline trajectory. To further simplify our analysis, we exclude the effects of gravity, surface wall, thermal radiation, chemical reaction of phases, and size distributions of solids and droplets. Heat transfer between gas and solids follows the lump heat capacity model, while heat transfer among solids and droplets occurs only by solids–droplets collisions, where solids are assumed to be trapped inside droplets upon collision.

2.1. Differential-integral governing equations

Governing equations of the flow mixing involves dynamic interactions among gas–solid–liquid three phases via the strong coupling of momentum, heat and mass transfer. The phase trajectory and mixing characteristics in the jet region can be readily described using the deterministic Lagrangian trajectory approach in a coordinate system (ξ, η) attached to the centerline of the jet, as shown in Fig. 1. All phases are assumed to be moving along the ξ direction only within the jet mixing region while the ambient gas and solids are engulfed into the mixing stream by jet entrainment. The jet mixing region is bended due to the convective as well as the collision mo-

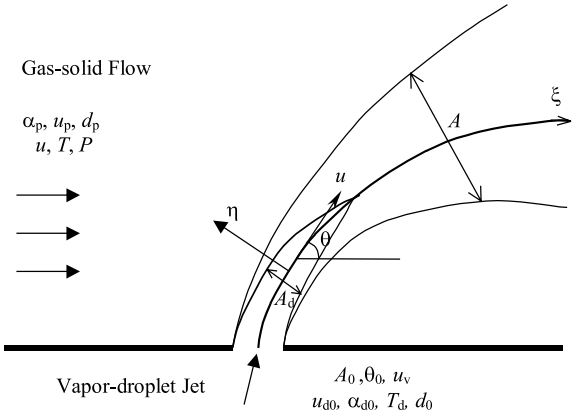

Fig. 1. Vapor–droplet spray jet in a uniform gas–solid flow.

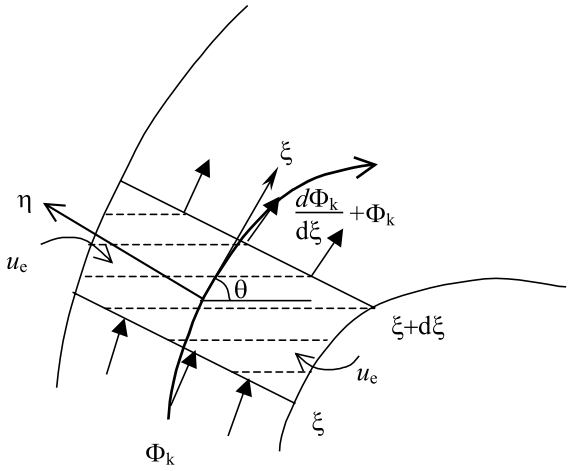

Fig. 2. Schematic diagram of control volume.

mentum transfer from flowing round gas–solid flow. Based on the mass, momentum, and energy balance over a control volume in the (ξ,η) coordinates, as shown in Fig. 2, general governing equations of each phase can be constructed in differential-integral forms. It is noted that, due to the assumption of the identical flow centerline of each phase in the mixing region, only one momentum equation in the η direction is independent. The most representative η-momentum equation should be selected from the phase whose inertia effect is the minimum among the three phases. Hence, in the following, the η-momentum equation of gas–vapor mixture is used to define the bending of the centerline.

2.1.1. Gas–vapor mixture phase

The continuity equation is derived based on a mass balance among the increase rate of mass flow along ξ, gas entrainment rate across the jet boundary, and vapor generation rate by droplet evaporation, which yields

$$\frac{\mathrm{d}}{\mathrm{d}\xi}\left[\int_A \rho_\mathrm{m} u\,\mathrm{d}A\right] = \alpha_\infty \rho_\infty u_\mathrm{e} \ell + \int_{A_\mathrm{d}} n_\mathrm{d} \dot{m}_\mathrm{e}\,\mathrm{d}A \tag{1}$$

where ρ_m and ρ_∞ are the density of gas–vapor mixture phase and density of ambient gas, respectively; u is the velocity of gas–vapor mixture phase while u_e is the gas entrainment velocity; A is the cross-sectional area of gas–vapor spray; α_∞ is the volume fraction of ambient gas; ℓ is the spray perimeter; n_d denotes the droplet number density; and $\dot{m}_\mathrm{e}$ stands for the mass generation rate per droplet.

The ξ-component momentum equation is obtained based on a ξ-component momentum balance among the increase rate of momentum flow, momentum entrainment carried by the gas entrainment across the jet boundary, momentum generation due to droplet evaporation, and interfacial momentum transfer between the mixture and droplets as well as between the mixture and solids. For simplicity, we may consider the Stokesian drag forces of individual droplets and

solids are the only forces responsible for the interfacial momentum transfer between the mixture and other two phases. Hence the ξ-component momentum equation is given by

$$\frac{\mathrm{d}}{\mathrm{d}\xi}\left[\int_A \rho_\mathrm{m} uu\,\mathrm{d}A\right] = \alpha_\infty \rho_\infty u_\mathrm{e} u_\infty \ell\cos\theta + \int_{A_\mathrm{d}} n_\mathrm{d}\dot{m}_\mathrm{e} u_\mathrm{d}\,\mathrm{d}A + \int_{A_\mathrm{d}} n_\mathrm{d} c_\mathrm{dd}\frac{\pi}{8} d_\mathrm{d}^2 \rho_\mathrm{m}(u_\mathrm{d}-u)^2\,\mathrm{d}A + \int_A n_\mathrm{p} c_\mathrm{dp}\frac{\pi}{8} d_\mathrm{p}^2 \rho_\mathrm{m}(u_\mathrm{p}-u)^2\,\mathrm{d}A \tag{2a}$$

where u_d and u_p stand for the velocity of droplets along with the jet trajectory and the velocity of particles, respectively; d_d is the diameter of a droplet; n_p is the particle number density; c_dd and c_dp represent respectively the drag coefficient of a droplet and the drag coefficient of a particle, which can be estimated by

$$c_\mathrm{dd} = \left(\frac{24}{Re_\mathrm{d}}\right)\left(1+\frac{1}{6}Re_\mathrm{d}^{2/3}\right), \qquad c_\mathrm{dp} = \left(\frac{24}{Re_\mathrm{p}}\right)\left(1+\frac{1}{6}Re_\mathrm{p}^{2/3}\right) \tag{2b}$$

as suggested by Putnam (1961).

The η-component momentum equation is developed based on a η-component momentum balance among the change rate of momentum, momentum entrainment carried by the gas entrainment, and drag forces from the gas–solid flow around the jet, which is expressed by

$$\frac{\mathrm{d}\theta}{\mathrm{d}\xi}\left[\int_A \rho_\mathrm{m} uu\,\mathrm{d}A\right] = -\alpha_\infty \rho_\infty u_\mathrm{e} u_\infty \ell\sin\theta - C_\mathrm{g} C_\mathrm{D}\sqrt{\frac{A}{\pi}}\alpha_\infty \rho_\infty u_\infty^2 \sin^2\theta - C_\mathrm{m}(1-\alpha_\infty)\rho_\mathrm{p} u_\mathrm{e}\ell u_{\mathrm{p}\infty}\sin\theta \tag{3a}$$

where C_D denotes the drag coefficient, which is estimated from a flow around a circular cylinder; C_g is a permeability correction factor of drag force for flow around the bending jet tube, which is approximated by the ratio of droplet mass flow rate to total jet mass flow rate; while C_m is a partition factor for momentum transfer by solids entrainment to the gas mixture. In this study,

$$C_\mathrm{D} = \begin{cases} 10 - 9\times 10^{-3} Re & 1 \leqslant Re \leqslant 10^3, \\ 1 & 10^3 \leqslant Re \leqslant 10^4, \end{cases} \qquad C_\mathrm{g} = \left(\frac{\rho_\mathrm{d} A_\mathrm{d}}{\rho A + \rho_\mathrm{d} A_\mathrm{d}}\right)^{0.25} \tag{3b}$$

The conservation of thermal energy is obtained based on the energy balance among the increase rate of flow enthalpy, the energy entrainment from the ambient gas stream, heat generation due to phase change, heat transfer between droplets and the mixture as well as the heat transfer between solids and the mixture, which is given by

$$\frac{\mathrm{d}}{\mathrm{d}\xi}\left[\int_A \rho_\mathrm{m} u c_\mathrm{p} T\,\mathrm{d}A\right] = \alpha_\infty \rho_\infty u_\mathrm{e} c_\mathrm{p} T_\infty \ell + \int_{A_\mathrm{d}} n_\mathrm{d}\dot{m}_\mathrm{e}(L + h_\mathrm{do})\,\mathrm{d}A + \int_{A_\mathrm{d}} n_\mathrm{d}\pi d_\mathrm{d}^2 h_\mathrm{d}(T_\mathrm{d}-T)\,\mathrm{d}A + \int_A (n_\mathrm{p} - f_\mathrm{dp})\pi d_\mathrm{p}^2 h_\mathrm{p}(T_\mathrm{p}-T)\,\mathrm{d}A \tag{4a}$$

where c_p is the thermal capacity of gas–vapor mixing phase; T, T_d and T_p represent respectively temperatures of the gas–vapor mixing phase, droplets and particles; h_d and h_p stand for the heat transfer coefficients of a single droplet and a single particle, respectively; and f_dp is the solids–droplets collision frequency. In the last term of right hand side of Eq. (4a), solids that collide with

droplets are excluded from the heat transfer process between solids and the mixture of gas and vapor. In this study, the effective heat transfer coefficient of a single droplet can be obtained from the effective Nusselt number, which is determined by Dwyer (1985)

$$Nu_{\mathrm{d}} = \frac{2 + 0.6Re_{\mathrm{d}}^{*0.5}Pr^{0.333}}{\left[1 + \frac{C_{\mathrm{p}}(T-T_{\mathrm{d}})}{L}\right]^{0.7}} \tag{4b}$$

where the relative Reynolds number of droplets in a gas–solids mixture is defined by

$$Re_{\mathrm{d}}^{*} = \frac{(\rho_{\mathrm{d}}\alpha_{\mathrm{d}} + \rho_{\mathrm{m}})(u_{\mathrm{d}} - u)d_{\mathrm{d}}}{\mu} \tag{4c}$$

The Nusselt number for the heat transfer coefficient of a single particle can be expressed by the Ranz–Marshall equation

$$Nu_{\mathrm{p}} = 2 + 0.6Re_{\mathrm{p}}^{0.5}Pr^{0.333} \tag{4d}$$

2.1.2. Droplet phase

Spray of fast evaporating liquids typically evaporates within the jet mixing region. The spray evaporation region is thus bounded within the jet mixing boundary. We assume only droplets on the outer boundary of the spray can get evaporated and the amount of droplets evaporated only depends on the amount of energy transferred into the spray region. For further simplicity, we only consider the straight sprays without spray divergence. The continuity equation is based on the fact that the decrease rate of mass flow along ξ is due to the droplet evaporation, which gives

$$\frac{\mathrm{d}}{\mathrm{d}\xi}\left[\int_{A_{\mathrm{d}}} \alpha_{\mathrm{d}}\rho_{\mathrm{d}}u_{\mathrm{d}}\,\mathrm{d}A\right] = -\int_{A_{\mathrm{d}}} n_{\mathrm{d}}\dot{m}_{\mathrm{e}}\,\mathrm{d}A \tag{5}$$

where A_{d} is the cross-sectional area of droplets jet; α_{d} is the volume fraction of droplets; and ρ_{d} stands for the density of droplets.

The ξ-component momentum equation is generated from a ξ-component momentum balance among the increase rate of droplet momentum flow, interfacial forces between droplets and the gaseous mixture, solids–droplets collision, and the momentum transfer due to droplet evaporation, which leads to

$$\begin{aligned}\frac{\mathrm{d}}{\mathrm{d}\xi}\left[\int_{A_{\mathrm{d}}} \alpha_{\mathrm{d}}\rho_{\mathrm{d}}u_{\mathrm{d}}u_{\mathrm{d}}\,\mathrm{d}A\right] = &-\int_{A_{\mathrm{d}}} n_{\mathrm{d}}c_{\mathrm{dd}}\frac{\pi}{8}d_{\mathrm{d}}^{2}\rho_{\mathrm{m}}(u_{\mathrm{d}} - u)^{2}\,\mathrm{d}A + \int_{A_{\mathrm{d}}} f_{\mathrm{dp}}\frac{\pi}{6}d_{\mathrm{p}}^{3}\rho_{\mathrm{p}}\left(u_{\mathrm{p}} - u_{\mathrm{d}}\right)\mathrm{d}A \\ &- \int_{A_{\mathrm{d}}} n_{\mathrm{d}}\dot{m}_{\mathrm{e}}u_{\mathrm{d}}\,\mathrm{d}A\end{aligned} \tag{6}$$

where ρ_{p} is the density of solid particles and u_{p} is the velocity of solid particles along with the trajectory.

The η-component momentum equation can be obtained based on a η-component momentum balance among the change rate of momentum and the momentum entrainment due to the solids entrainment, which gives

$$\frac{\mathrm{d}\theta}{\mathrm{d}\xi}\left[\int_{A_\mathrm{d}} \alpha_\mathrm{d}\rho_\mathrm{d}u_\mathrm{d}u_\mathrm{d}\,\mathrm{d}A\right] = -(1-C_\mathrm{m})(1-\alpha_\infty)\rho_\mathrm{p}u_\mathrm{e}\ell u_{\mathrm{p}\infty}\sin\theta \tag{7}$$

It is noted that Eqs. (7), (3a) and (3b) are not independent from each other due to the previous assumption on the same centerline of all phases. Nevertheless, by solving the derivative term from Eqs. (3a), (3b) and (7) can be regarded as an equation to estimate the partition factor C_m. An energy balance is established among the increase rate of flow enthalpy of droplets, heat convection from the gaseous mixture, heat transfer from solids by collision, and the latent heat transfer due to droplet evaporation. Thus the energy equation of droplets is obtained by

$$\begin{aligned}\frac{\mathrm{d}}{\mathrm{d}\xi}\left[\int_{A_\mathrm{d}} \alpha_\mathrm{d}\rho_\mathrm{d}u_\mathrm{d}c_\mathrm{pd}T_\mathrm{d}\,\mathrm{d}A\right] &= \int_{A_\mathrm{d}} \pi n_\mathrm{d}d_\mathrm{d}^2h_\mathrm{d}(T-T_\mathrm{d})\,\mathrm{d}A - \int_{A_\mathrm{d}} n_\mathrm{d}\dot{m}_\mathrm{e}(L+h_\mathrm{do})\,\mathrm{d}A \\ &\quad + \int_{A_\mathrm{d}} f_\mathrm{dp}\frac{\pi}{6}d_\mathrm{p}^3\rho_\mathrm{p}c_\mathrm{pp}\left(T_\mathrm{p}-T_\mathrm{d}\right)\mathrm{d}A\end{aligned} \tag{8}$$

where c_pd is the thermal capacity of liquid droplets while c_pp is the thermal capacity of solid particles.

2.1.3. Solids phase

It is assumed that solids enter the mixing region only by jet entrainment and all entrained solids flow along the ξ-direction only. Once solids collide with a droplet, they remain trapped until the host droplet is completely evaporated. The effect of the solids reoccurrence from evaporated droplets is neglected. Thus the mass balance equations is obtained by

$$\frac{\mathrm{d}}{\mathrm{d}\xi}\left[\int_{A} \alpha_\mathrm{p}\rho_\mathrm{p}u_\mathrm{p}\,\mathrm{d}A\right] = (1-\alpha_\infty)\rho_\mathrm{p}u_\mathrm{ep}\ell \tag{9}$$

where u_ep represents the entrainment velocity of solid particle.

The momentum equation is obtained based a momentum balance among the increase rate of solids momentum flow, momentum transfer by solids entrainment, interfacial forces from the gaseous mixture, and momentum changes due to solids–droplets collision, which is expressed by

$$\begin{aligned}\frac{\mathrm{d}}{\mathrm{d}\xi}\left[\int_{A} \alpha_\mathrm{p}\rho_\mathrm{p}u_\mathrm{p}u_\mathrm{p}\,\mathrm{d}A\right] &= (1-\alpha_\infty)\rho_\mathrm{p}u_\mathrm{ep}\ell u_{\mathrm{p}\infty}\cos\theta - \int_{A_\mathrm{d}} f_\mathrm{dp}\frac{\pi}{6}d_\mathrm{p}^3\rho_\mathrm{p}\left(u_\mathrm{p}-u_\mathrm{d}\right)\mathrm{d}A \\ &\quad - \int_{A} n_\mathrm{p}c_\mathrm{dp}\frac{\pi}{8}d_\mathrm{p}^2\rho_\mathrm{m}\left(u_\mathrm{p}-u\right)^2\mathrm{d}A\end{aligned} \tag{10}$$

In this modeling approach, we assume that all entrained solids flow along the ξ-direction only and the η-component entrained momentum from the solids entrainment has been partitioned to the gas-mixture via interfacial forces and to the droplet phase via collision. Therefore, there is no η-component momentum equation for the solids phase. The energy equation of solids phase is based on an energy balance among the increase rate of flow enthalpy of solids, heat transfer from the solids entrainment, heat transfer by droplets–solids collision, and heat transfer between solids and gaseous mixture, which gives

$$\frac{\mathrm{d}}{\mathrm{d}\xi}\left[\int_A \alpha_\mathrm{p}\rho_\mathrm{p}u_\mathrm{p}c_\mathrm{pp}T_\mathrm{p}\,\mathrm{d}A\right] = \alpha_{\mathrm{p}\infty}\rho_\mathrm{p}u_\mathrm{ep}c_\mathrm{pp}T_{\mathrm{p}\infty}\ell - \int_{A_\mathrm{d}} f_\mathrm{dp}\frac{\pi}{6}d_\mathrm{p}^3\rho_\mathrm{p}c_\mathrm{pp}\left(T_\mathrm{p}-T_\mathrm{d}\right)\mathrm{d}A - \int_A (n_\mathrm{p}-f_\mathrm{dp})\pi d_\mathrm{p}^2 h_\mathrm{p}\left(T_\mathrm{p}-T\right)\mathrm{d}A \tag{11}$$

2.1.4. Problem closure

An additional equation is needed to closure the problem. We apply the equation of state of ideal gas to the gas–vapor mixture to yield

$$\rho_\mathrm{m} = (1-\alpha_\mathrm{p}-\alpha_\mathrm{d})\frac{P}{RT} \tag{12}$$

So far we have obtained 11 coupled independent equations (from Eqs. (1)–(12), except for (7)) for solving 11 independent variables $(A, A_\mathrm{d}, \theta, \rho_\mathrm{m}, \alpha_\mathrm{p}, \dot{m}_\mathrm{e}, u, u_\mathrm{d}, u_\mathrm{p}, T, T_\mathrm{p})$. The problem in principle is closed. Hence, with the given or presumed cross-sectional distributions for variables of interest, the coupled differential-integral equations become solvable.

2.1.5. Intrinsic correlation

In order to solve the governing equations, additional intrinsic correlations on the flow entrainment velocity, particle collision frequency and collision efficiency must be provided. Although we realize that the presence of particles and droplets in the jet flow does affect the flow entrainment, there is no simple correlation to quantify this effect. In this model, we use the equation of jet entrainment velocity in single-phase flows, which was proposed by Platten and Keffer (1968), as our first-order approximation. Hence, the flow entrainment velocity is estimated by

$$u_\mathrm{e} = 0.06(u - u_\infty\cos\theta) + 0.3u_\infty(\cos\theta - \cos\theta_0) \tag{13a}$$

A similar equation is extended to estimate the jet entrainment of particle phase so that

$$u_\mathrm{ep} = 0.06(u_\mathrm{p} - u_{\mathrm{p}\infty}\cos\theta) + 0.3u_{\mathrm{p}\infty}(\cos\theta - \cos\theta_0) \tag{13b}$$

Although the above entrainment velocity was originally obtained from the study of oblique jets, the extension of this equation to a co-current case reveals a close resembling of the equations directly derived from co-current jet studies, for example, $u_\mathrm{e} = 0.026(u - u_\infty)$ from Rajaratnam (1976). For simplicity and generality of our mechanistic modeling, we adopt Eqs. (13a) and (13b) as a general one to cover all injection angles.

Collision frequency among droplets and solid particles can be calculated by Fan and Zhu (1998)

$$f_\mathrm{dp} = \eta_\mathrm{co}n_\mathrm{d}n_\mathrm{p}\frac{\pi\left(d_\mathrm{p}+d_\mathrm{d}\right)^2}{4}|u_\mathrm{p}-u_\mathrm{d}| \tag{14}$$

where the collision efficiency, η_co, is given from an analytical approximation, which is derived based on the rigid sphere collisions in Stokesian flows (Zhu, 2000)

$$\eta_{co} = \left(1 + 34\frac{d_d}{d_p}\frac{\rho}{\rho_p}\frac{1}{Re_{pd}}\right)^{-2} \tag{15}$$

where Re_{pd} is the particle Reynolds number based on the relative velocity of particle and droplet.

3. Experimental study

Our previous experimental investigation was conducted for spray jetting in a co-current gas–solid flow (Zhu et al., 2000). In this study, we extend the measurements into a study of oblique jets with inclined angles of injections. The experimental apparatus is schematically shown in Fig. 3. An induced fan provides the needed power of the pipe flow while a screw-driven powder feeder feeds dry powder into the airflow to generate a continuous gas–solid suspension flow. The solid phase consists of solid particles of 70 μm in mean diameter and 1200 kg/m^3 in density. A pressure-regulator controlled liquid nitrogen jet system is used to generate the evaporating jet spray that is introduced into the gas–solid suspension flow at room temperature. The mass feeding rate of liquid nitrogen is measured by an in-site electronic balance (BP2100, Sartorius).

Major characteristic parameters to be experimentally investigated include jet evaporation length and jet flow pattern. The evaporation length is measured using a temperature measurement system (to take advantage of latent heat involved in evaporation) while the jet flow pattern is visualized by a laser-sheet assisted flow visualization system (Zhu et al., 2000). An Argon ion laser

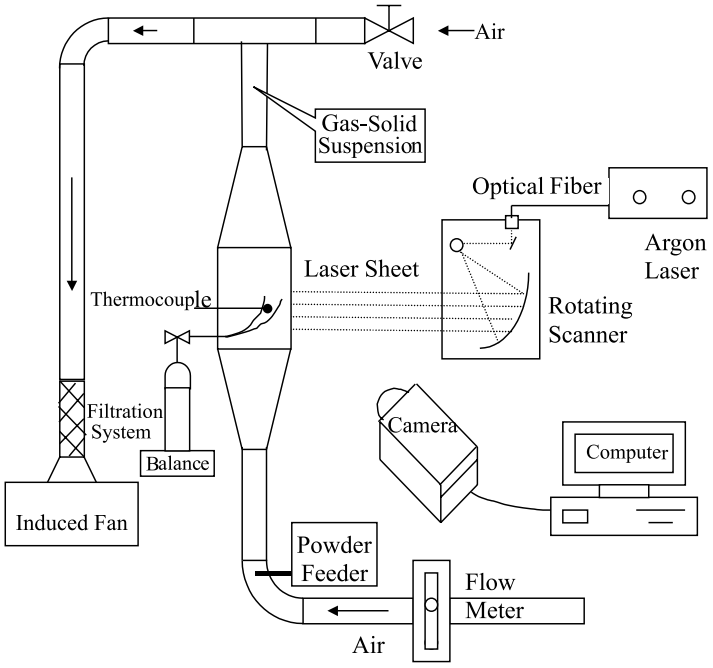

Fig. 3. Experimental system.

(Reliant 1000M, Laser Physics) is used in connection with the laser sheet generation device, producing a pseudo laser sheet with a laser beam sweeping within a range of 500 mm at a frequency up to 500 Hz. The digitized images of spray and flowing solids are then captured by a CCD camera (Megaplus ES310, Kodak) and analyzed by the EPIX digital analysis system.

4. Results and discussion

Based on the proposed parametric model, various parametric effects such as particle volume fraction on jet evaporation and effect of injection angle on jet trajectory have been investigated. In

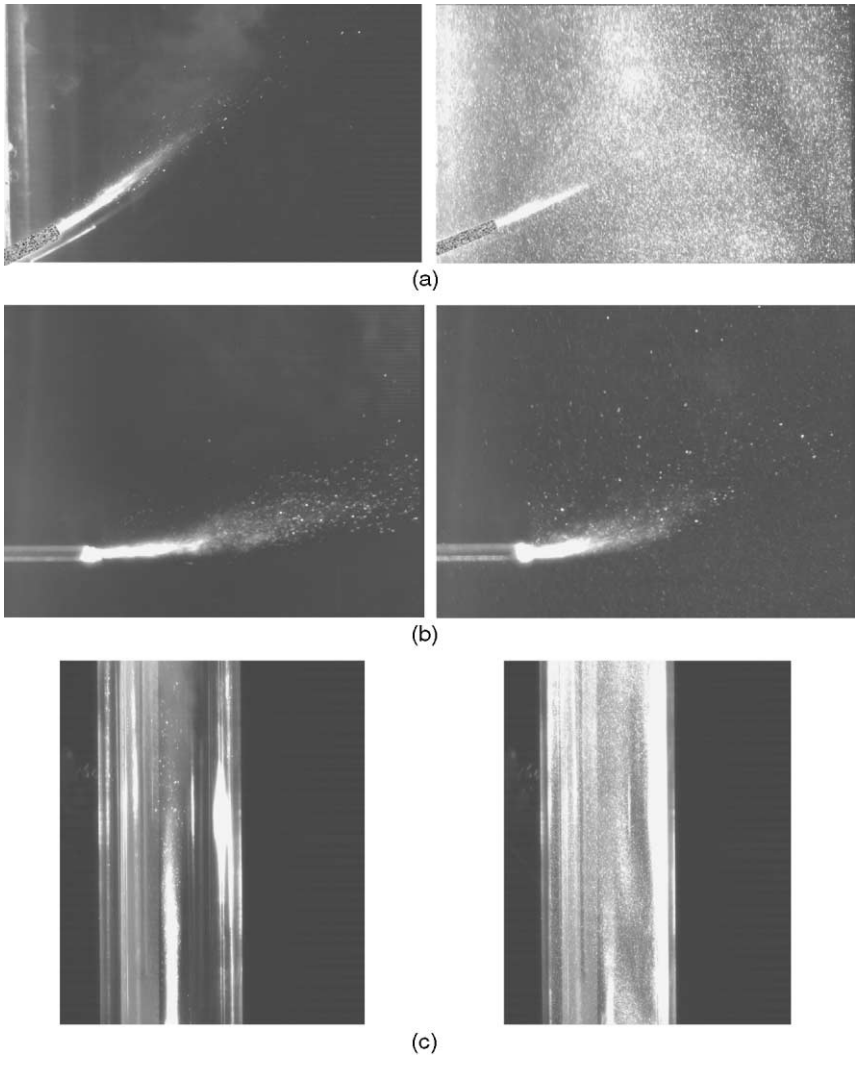

Fig. 4. Effect of solids on jet evaporation without and with solid particles. (a) Oblique-flow jet at injection angle of 60°. (b) Cross-flow jet. (c) Co-current flow jet.

this paper, in order to make a comparison with our experimental results, sample calculations are performed for liquid nitrogen spray jets in air-FCC flows.

4.1. Effects of solids loading on jet evaporation

Our previous experimental study showed that the presence of solid particles can significantly reduce the jet evaporation length in a co-current gas–solid flow (Zhu et al., 2000). In this study, we extend the measurements into a study of oblique and cross-flow jets with inclined angles of injections. The experimental results, illustrated in Fig. 4, show that the presence of solid particles indeed significantly reduce the jet evaporation length not only in a co-current jet spray but also in cross-flow jet and other oblique spray cases. To enhance the visual effect and smooth out the jet fluctuations, 15 successive images are overlapped, which are shown in Fig. 4(a) and (b). In Fig. 4(a), the solids volumetric concentration is about 0.2% while in Fig. 4(b), it is about 0.05%. The solids concentration in Fig. 4(c) is about 1%. The difference in solids volume fraction in co-current jet and cross-flow jet is due to the geometric limitations of test sections for the respective tests. The effect of solids on jet evaporation length can be expected because, with the presence of solid particles, the liquid spray jets acquire much more heat through the collision between particles and droplets, and hence the droplets evaporate quicker than that in particle-free flows. As an effort of modeling validation, a quantitative comparison between the measurements and modeling predictions is made for the co-current spray case, as shown in Fig. 5, which suggests a fairly good agreement on the trend of the effect of solids volumetric loading and hence partially validates our parametric model efforts. Fig. 6 illustrates the effect of solid loading on jet evaporation length for both co-current and cross-flow spray jets, which shows that the jet evaporation lengths in both cases are significantly shortened. Cross-flow spray evaporates faster than the co-current spray due to the convection of solids and ambient gas stream. It is interesting to note that, with the increase

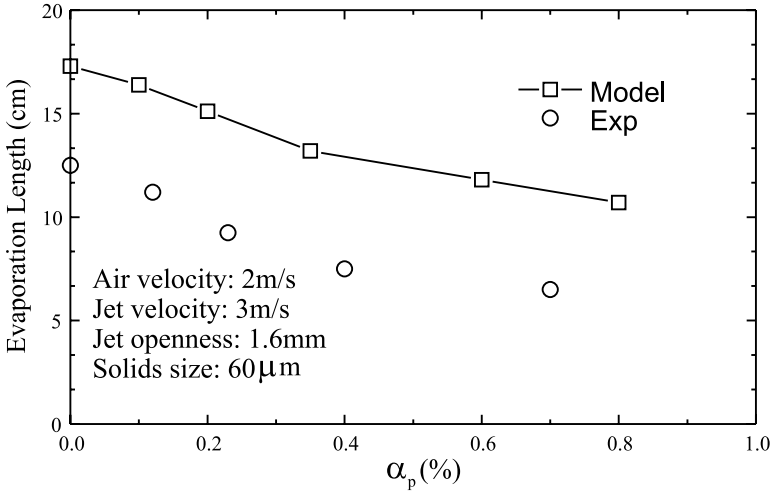

Fig. 5. Effect of particle loading on jet evaporation length.

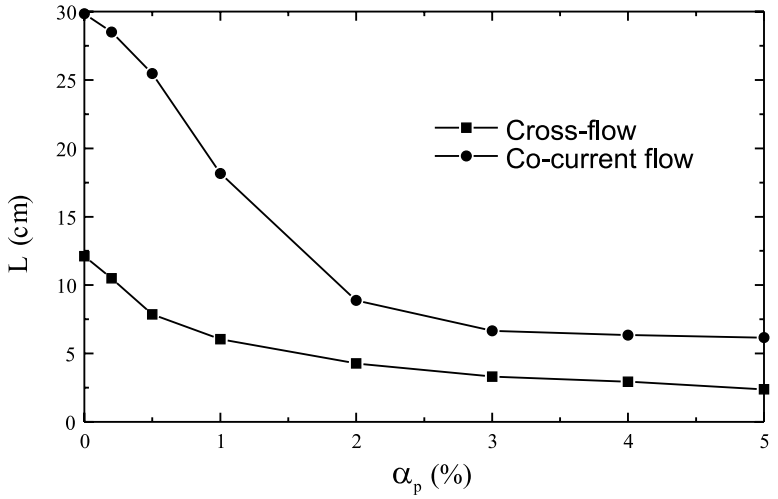

Fig. 6. Comparison of evaporation length between co-current and cross-flow jets.

of solids loading, the evaporation length decreases asymptotically. The vapors, fast evaporated due to drop-solid collision, will push the solids out of the evaporation region. The more solids loading, the more evaporation vapors, the more push. This means the increase of solids concentration in the spray region does not have the same rate in the ambient region. Therefore, with the increase of solids loading, a balance condition should be achieved It is noted that the jet-induced entrainment is reduced by the droplet evaporation. With the increase of solids loading, more solids would be entrained into the spray region, leading to an increase in spray evaporation. However the increased evaporation in turn would lead to a reduction in entrainment rate of solids. Hence, an asymptotic trend of spray evaporation length is resulted, with the increase of solids loading. In this example, significant reductions of evaporation lengths occur within a solids volumetric loading of 1%.

4.2. Effect of injection angle on spray trajectory

As indicated in Fig. 6, spray injection angle can have a strong influence on spray trajectory and evaporation rate. This is because the spray trajectory is heavily dependent on the drag forces from the air stream and the collision forces from the solids phase, which varies at different spray injection angle under otherwise the same conditions. The heat transfer, a vital factor for the droplet evaporation, is dominated by heat convection of gas flowing around droplets and heat conduction upon solids-droplet collisions. Both heat transfer mechanisms are injection angle dependent. Fig. 7 shows a typical effect of injection angle on spray trajectory and evaporation length, which indicates a longer evaporation length at a smaller injection angle towards the co-current jet spray. This is due to the fact that, with the increase of jet incident angle, the entrainment amount of both solid particles and air gas increases, and, at the same time, the convection effect becomes increasingly important, which leads more heat transfer to liquid droplets and accelerates the evaporation of droplets.

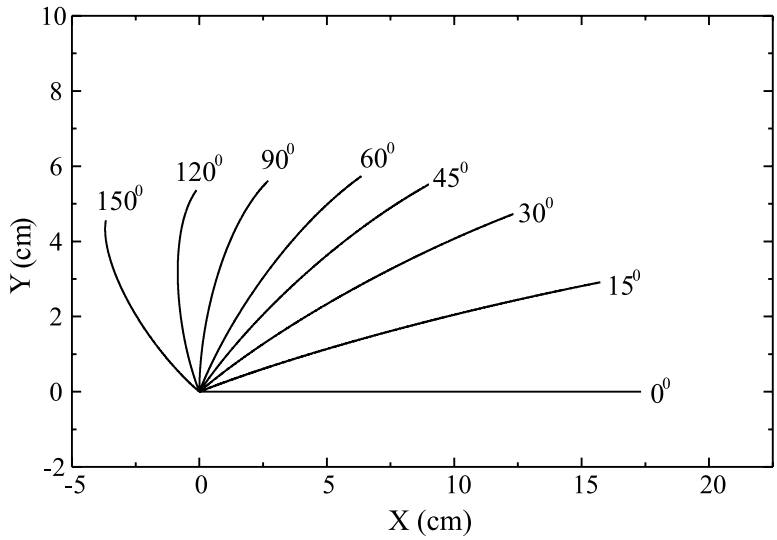

Fig. 7. Effect of jet injection angle on droplets trajectory and evaporation length.

4.3. Dilution effects by evaporation

Droplet evaporation in gas–solid flows leads to the dilution effects on solids concentration as well as temperature reduction of all phases in the spray evaporation region. Fig. 8 shows a velocity distribution of the gas–vapor mixture along the jet trajectory. As shown in Fig. 8, the gas phase velocity is above the ambient velocity within the evaporation region, due to the addition of vapor by droplets evaporation as well as the initial injection velocity. The gas velocity reduces quickly

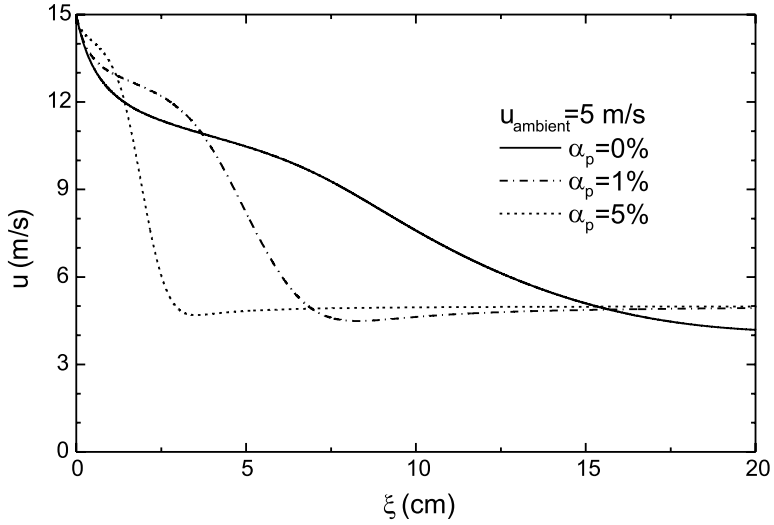

Fig. 8. Gas velocity distribution along with jet trajectory in a cross-flow jet.

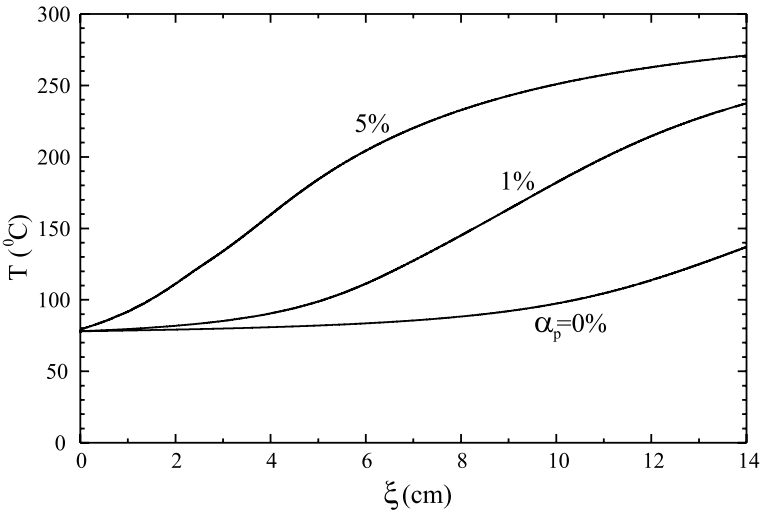

Fig. 9. Gas temperature distribution along jet tractory in a cross-flow jet.

along with the jet trajectory by the quick reduction of the evaporation rate. Fig. 8 also illustrates the effect of solid loadings on the velocity distribution. The higher the solids loading the quicker the velocity reduction. This is because a higher solids loading means more solid particles entrained into the spray evaporation region, which leads to an increased drag force to the gas phase. When the gas velocity decreases to a level below the ambient velocity of gas–solid suspension, the gas velocity in the evaporation region intends to increase due to the effect of momentum transfers across the jet boundary. Consequently, the gas velocity approaches asymptotically to the ambient value.

The gas temperature distribution along with the jet trajectory, at different solid loadings, is shown in Fig. 9. The temperature dilution effect is reflected in Fig. 9 by the fact that the gas temperature in the evaporation region is always below the ambient value. The higher the solids loading the quicker increase in the gas temperature since the higher solid loading contributes more heat to droplet vaporization and gas–vapor mixture.

5. Conclusions

A parametric model has been developed for study of liquid jet evaporation in gas–solid suspension flows, which includes all phase interactions with phase changes in the three phases. Parametric effects on the mixing characteristics such as evaporation length, temperature and velocity of each phase, trajectories, and the phase volume fraction distributions are illustrated. It is found that the evaporation length is shortened in the presence of particles in a liquid jet of any injection angle. The evaporation length decreases with the increase of solids loading as well as the increase of jetting angle from co-current to counter-current. Effect of a jet incident angle is also investigated. The comparison between the model predictions and experiments in the co-current spray case illustrates a good qualitative agreement.

Acknowledgements

Acknowledgement is made to Donors of The Petroleum Research Fund, administered by the American Chemical Society, for partial support of this research under the grant of ACS-PRF#35514-AC9.

References

Abramovich, G.N., 1963. The theory of turbulent jets. M.I.T. Press, MA (English translation).

Campbell, J.F., Schetz, J.A., 1973. Flow properties of submerged heated effluents in a waterway. AIAA Journal 15, 223–230.

Chang, S.L., Lottes, S.A., Zhou, C.Q., Golchert, B., Petrick, M., 1998. Interactions of multi-phase hydrodynamics, droplet evaporation, and chemical kinetics in FCC riser reactors. AIAA/ASME Joint Thermophysics and Heat Transfer Conference 1, 261.

Chen, T.H., Roe, L.A., Nejad, A.S., 1994. Multifunction droplet imaging and velocimetry system for spray jets. Journal of Propulsion and Power 10 (6), 798–803.

Dwyer, H.A., 1985. Progress Energy Combustion Science 15, 131.

D'souza, R., Forney, L.J., 1990. Slow bimolecular reactions in a deflected turbulent jet. The Chemical Engineering Journal 43, 127–136.

Edelman, R.B., Economos, C., Boccro, J., 1971. AIAA Journal 9, 1935–1940.

Field, M.A., 1963. Entrainment into an air jet laden with particles. BCURA Inf., p. 273.

Fan, L.-S., Zhu, C., 1998. In: Principles of Gas–Solid Flows. Cambridge University Press, Cambridge, p. 172.

Forney, L.J., Kwon, T.C., 1979. Efficient single-jet mixing in turbulent tube flow. AIChE Journal 25 (40), 623–630.

Han, K.S., Chung, M.K., 1992a. Numerical simulation of a two-phase gas-particle jet in a crossflow. Aerosol Science and Technology 16, 126–139.

Han, K.S., Chung, M.K., 1992b. Numerical simulation of a two-phase gas-particle jet in a crossflow, part 2. Free stream velocity gradient and heat transfer mechanism. Aerosol Science and Technology 17, 59–68.

Li, H.S., Karagozian, A.R., 1990. Breakup of a liquid jet in supersonic crossflow. AIAA Journal 30, 1919–1921.

Newton, D., 1998. How BP makes use of its X-ray imaging facility to support developments in fluidized bed processes. Proceedings of 1998 AIChE annual Meeting, p. 221.

Platten, J.L., Keffer, J.F., 1968. Entrainment in deflected axisymmetric jets at various angles to the stream. Tech. Rep. 6808, Department of Mechanical Engineering, University of Toronto.

Putnam, A., 1961. Integrable form of droplet drag coefficient. ARS Journal 31, 1467–1468.

Rajaratnam, N., 1976. Turbulent Jets. Elsevier Science, Amsterdam (Chapter 9).

Ricou, F.P., Spalding, D.B., 1961. Measurements of entrainment by axisymmetrical turbulent jets. Journal of Fluid Mechanics 11, 21–32.

Rudinger, G., 1975. Some aspects of gas-particle jets in a cross flow. ASME Paper 75-WA/HT-5.

Salzman, R.N., Schwartz, S.H., 1978. Transactions of the ASME, Journal of Fluids Engineering 100, 333–339.

Skouby, D.C., 1998. Hydrodynamics studies in a 0.45-m riser with liquid feed injection. Proceedings of 1998 AIChE Annual Meeting, p. 238.

Subramanian, V., Ganesh, R., 1982. Entrainment by a concentric jet with particles in the secondary stream. Canadian Journal of Chemical Engineering 60, 589–592.

Subramanian, V., Ganesh, R., 1984. Influence of free stream velocity on the entrainment by single- and two-phase axi-symmetric jet. AIChE Journal 30, 1010–1013.

Subramanian, V., Venkatram, S., 1985. Particle entrainment by axi-symmetric jets. The Canadian Journal of Chemical Engineering 63, 853–855.

Tatterson, D.F., Marker, T.L., Forgac, J.M., 1987. Particle effects on free jet entrainment. The Canadian Journal of Chemical Engineering 65, 361–365.

Wu, P.K., Kirkendall, K.A., Fuller, R.P., 1998. Spray structures of liquid jets atomized in subsonic crossflows. Journal of Propulsion and Power 14 (2), 173–182.

Zhu, C., 2000. Wet rotating granular filter for fine particulate filtration. Progress report to NJCST-PPRC.
Zhu, C., Wang, X., Fan, L.-S., 2000. Effect of solids concentration on evaporative liquid jets in gas–solid flows. Powder Technology 111, 79–82.
Zhu, C., Wang, X., Liu, G., Fan, L.-S., 2001. A similarity model of evaporating liquid spray jets in concurrent gas–solid flows. Powder Technology 119, 292–297.